

THE TRANSPORT OF IMAGES METHOD: COMPUTING ALL ZEROS OF HARMONIC MAPPINGS BY CONTINUATION

Olivier Sète* Jan Zur*

October 30, 2020

Abstract

We present a novel continuation method to compute all zeros of a harmonic mapping f in the complex plane. Our method works without any prior knowledge about the number of zeros, or their approximate location, as long as the number of zeros is finite. We give a complete convergence analysis, which relies on results on the caustics of f , and on convergence results for Newton's method. In our numerical examples, the method terminates with the correct number of zeros, is very fast compared to general purpose root finders, and is highly accurate in terms of the residual. An easy-to-use Matlab implementation of our method is freely available online.

Keywords: Harmonic mappings, continuation method, root finding, zeros, Newton's method, critical curves and caustics.

AMS Subject Classification (2010): 65H20; 31A05; 30C55.

1 Introduction

We study the zeros of harmonic mappings, i.e., $f : \Omega \rightarrow \mathbb{C}$ with $\Delta f = 0$ on an open subset Ω of \mathbb{C} . These functions have a local decomposition

$$f(z) = h(z) + \overline{g(z)} \quad (1.1)$$

with analytic h, g , but are themselves non-analytic in general. Several results on the number of zeros for special classes of harmonic mappings are known in the literature, e.g., for harmonic polynomials, i.e., $f(z) = p(z) + \overline{q(z)}$, where p and q are analytic polynomials [35, 15, 9, 16], for rational harmonic

*TU Berlin, Department of Mathematics, MA 3-3, Straße des 17. Juni 136, 10623 Berlin, Germany. {sete,zur}@math.tu-berlin.de

mappings of the form $f(z) = r(z) - \bar{z}$, where r is a rational function [13, 5, 19, 20, 27, 26, 17, 18, 28], or certain transcendental harmonic mappings [8, 4, 12].

While the above publications have a theoretical focus, we are here interested in the numerical computation of the zeros of f . A *single* zero can be computed by an iterative root finder, e.g., Newton's method on \mathbb{R}^2 (see [29] for a convenient formulation for harmonic mappings). The computation of *all* zeros is much more challenging. Of course, one could focus on certain regions in the complex plane and run the root finder with multiple starting points. The problem with such an approach is, however, that in general the number of zeros of harmonic mappings is not known a priori. In fact, even for harmonic polynomials $f(z) = p(z) - \bar{z}$ with $\deg(p) = n \geq 2$, the number of zeros can vary between n and $3n - 2$, and all these different numbers of zeros are attained by some harmonic polynomial; see [28, Thm. 5.4].

In this paper we derive a novel method to compute all zeros of a (non-degenerate) harmonic mapping, provided that the number of zeros is finite. We are not aware of any specialized method for this problem in the literature. Our method works without any prior knowledge about the number of these zeros, or their approximate location in the complex plane. It is based on continuation and prediction-correction, a general scheme which has been successfully applied for the numerical solution of systems of nonlinear equations and other problems; see, e.g., [1]. The overall idea is as follows: We first observe that for $\eta \in \mathbb{C}$ with $|\eta|$ large enough, the zeros of $f(z) - \eta$ are close to the poles of f , and these poles are usually known a priori. We thus are able to solve $f(z) = \eta_1$ for a large $|\eta_1|$. We then construct a sequence η_2, η_3, \dots using a prediction-correction scheme, and solve $f(z) = \eta_{k+1}$ based on the solutions for η_k . We let this sequence tend towards the origin and eventually, after finitely many steps, we end with $\eta_n = 0$, so that by solving $f(z) = \eta_n$ we obtain (numerically) all zeros of f .

The theoretical foundation of the *transport of images method* uses results of Lyzzaik [21], Neumann [23] and our previous results in [29, 28]. We prove that our method is guaranteed to compute all zeros of a non-degenerate harmonic mapping f . A key ingredient is the correct handling of turning points of the homotopy curves in the continuation method described above. During the iteration, the number of solutions of $f(z) = \eta_k$ and $f(z) = \eta_{k+1}$ can differ. This effect depends on the caustics of f (curves of the critical values). More precisely, the number of solutions of $f(z) = \eta$ changes by ± 2 when η changes from one side to the other of a single caustic arc [28]. For every step from η_k to η_{k+1} , we construct a (minimal) set of points S_{k+1} , such that all solutions of $f(z) = \eta_{k+1}$ are obtained by applying Newton's method with initial points from S_{k+1} .

Our numerical examples highlight three key features of our method: (1) it terminates with the correct number of zeros, (2) it is significantly faster

than methods that are not problem adapted, such as Chebfun2¹, and (3) it is highly accurate in terms of the residual. An easy-to-use Matlab implementation² is freely available online.

The name of the transport of images method is borrowed from astrophysics. In [25, Sect. 10.5], the idea is roughly described in the context of gravitational lensing. There, the parameter η models the position of a far away light source, and its lensed images are represented by the solutions of $f(z) = \eta$ with a harmonic mapping f ; see the surveys [14, 24, 3]. However, the description in [25] lacks many details and contains no convergence analysis.

Our paper is organized as follows. We recall relevant results on harmonic mappings in Section 2. In Section 3 we study the transport of images method, and investigate the solution curves of $f(z) = \eta(t)$ depending on t . Key aspects of our implementation are discussed in Section 4. In Section 5 we illustrate our method with several numerical examples using our Matlab toolbox. We close with concluding remarks and a brief outlook in Section 6.

2 Preliminaries

We briefly present relevant results for the computation of all zeros of harmonic mappings, following the lines of [28] and [21].

2.1 Decomposition of harmonic mappings

Let $\Omega \subseteq \mathbb{C}$ be open and connected. A *harmonic mapping* on Ω is a function $f : \Omega \rightarrow \mathbb{C}$ with $\Delta f = 4\partial_{\bar{z}}\partial_z f = 0$, where ∂_z and $\partial_{\bar{z}}$ denote the *Wirtinger derivatives*. If f is harmonic in the open disk $D_r(z_0) = \{z \in \mathbb{C} : |z - z_0| < r\}$, it has a local decomposition

$$f(z) = h(z) + \overline{g(z)} = \sum_{k=0}^{\infty} a_k(z - z_0)^k + \overline{\sum_{k=0}^{\infty} b_k(z - z_0)^k}, \quad z \in D_r(z_0), \quad (2.1)$$

with analytic functions h and g in $D_r(z_0)$, which are unique up to an additive constant; see [7, p. 412] or [6, p. 7]. If f is harmonic in the punctured disk $D = \{z \in \mathbb{C} : 0 < |z - z_0| < r\}$, i.e., z_0 is an isolated singularity of f , then

$$f(z) = \sum_{k=-\infty}^{\infty} a_k(z - z_0)^k + \overline{\sum_{k=-\infty}^{\infty} b_k(z - z_0)^k} + 2A \log|z - z_0|, \quad z \in D; \quad (2.2)$$

see [32, 10, 2]. The point z_0 is a *pole* of f , if $\lim_{z \rightarrow z_0} f(z) = \infty$, and an *essential singularity*, if the limit does not exist in $\widehat{\mathbb{C}} = \mathbb{C} \cup \{\infty\}$; see [30,

¹Chebfun2, www.chebfun.org, version of September 30, 2020.

²Transport of images toolbox, <https://github.com/transportofimages/>.

p. 44], [32, Def. 2.1] or [28, Def. 2.9]. It is possible that f has a pole at z_0 , but both series in (2.2) have an essential singularity at z_0 , as the example $f(z) = z^{-2} + \cos(i/z) + \overline{\cos(i/z)}$ from [32, Ex. 2.3] shows. It is also possible that f has an essential singularity at z_0 , but both series have a pole at z_0 , as shown by $f(z) = z^{-1} + \bar{z}^{-1}$.

The next proposition is the analog of the well-known facts, that a function holomorphic on $\widehat{\mathbb{C}}$ is constant, and a function meromorphic on $\widehat{\mathbb{C}}$ is rational.

Proposition 2.1. *A harmonic mapping f on $\widehat{\mathbb{C}} \setminus \{z_1, \dots, z_m\}$ with poles at $z_1, \dots, z_m \in \widehat{\mathbb{C}}$, at which the principal parts of both series in the decomposition (2.2) have only finitely many terms, has the form*

$$f(z) = r(z) + \overline{s(z)} + \sum_{j=1}^m 2A_j \log|z - z_j|, \quad (2.3)$$

where $A_1, \dots, A_m \in \mathbb{C}$, and r and s are rational functions which can have poles only at z_1, \dots, z_m . If some $z_j = \infty$, then $\log|z|$ replaces $\log|z - z_j|$. In particular, if f is harmonic on $\widehat{\mathbb{C}}$, then f is constant.

Proof. First, let f be a harmonic mapping on $\widehat{\mathbb{C}}$. Then $\partial_z f$ is analytic on $\widehat{\mathbb{C}}$ and thus constant [34, Thm 3.5.8]. Let $h' = \partial_z f$, then $h(z) = a_1 z + a_0$ is analytic. Let $g = \overline{f - h}$. Since $\partial_{\bar{z}} g = \overline{\partial_z f - h'} = 0$, g is analytic on $\widehat{\mathbb{C}}$ and hence constant, say $g(z) = b_0$, and we have $f(z) = a_1 z + a_0 + \bar{b}_0$. Since f is harmonic at ∞ , we have $a_1 = 0$ and f is constant. Next, let f be harmonic with poles at z_1, \dots, z_m . If $z_j \neq \infty$, the decomposition (2.2) has the form

$$f(z) = \sum_{k=-n}^{\infty} (a_k(z - z_j)^k + \overline{b_k(z - z_j)^k}) + 2A_j \log|z - z_j|,$$

and we set $f_j(z) = \sum_{k=-n}^{-1} (a_k(z - z_j)^k + \overline{b_k(z - z_j)^k}) + 2A_j \log|z - z_j|$. Similarly, if $z_j = \infty$. Then $f - f_1 - \dots - f_m$ has removable singularities at z_1, \dots, z_m , and can be extended to a harmonic mapping in $\widehat{\mathbb{C}}$ (see [28, p. 8], or also [11, Thm. 15.3d]), which is constant. \square

2.2 Critical set and caustics of harmonic mappings

The critical points of a harmonic mapping $f : \Omega \rightarrow \mathbb{C}$, i.e., the points where the *Jacobian* of f ,

$$J_f(z) = |\partial_z f(z)|^2 - |\partial_{\bar{z}} f(z)|^2, \quad (2.4)$$

vanishes, form the *critical set* of f ,

$$\mathcal{C} = \{z \in \Omega : J_f(z) = 0\}. \quad (2.5)$$

By Lewy's theorem [6, p. 20], f is locally univalent at $z \in \Omega$ if, and only if, $z \notin \mathcal{C}$. Here and in the following, we assume that $\partial_z f$ and $\partial_{\bar{z}} f$ do not vanish

identically, otherwise f would be analytic or anti-analytic, which is not the focus of this paper. Then $\partial_z f$ has only isolated zeros in Ω , and the critical set consists of isolated points and a level set of the *second complex dilatation* of f ,

$$\omega(z) = \frac{\overline{\partial_{\bar{z}} f(z)}}{\partial_z f(z)}, \quad (2.6)$$

which is a meromorphic function in Ω . We assume that removable singularities of ω in Ω are removed. Let

$$\mathcal{M} = \{z \in \mathcal{C} : |\omega(z)| \neq 1\} \quad (2.7)$$

$$= \{z \in \Omega : \partial_z f(z) = \partial_{\bar{z}} f(z) = 0 \text{ and } \lim_{\zeta \rightarrow z} |\omega(\zeta)| \neq 1\}, \quad (2.8)$$

see [28, p. 4], which consists of isolated points of \mathcal{C} [21, Lem. 2.2], then

$$\mathcal{C} \setminus \mathcal{M} = \{z \in \Omega : |\omega(z)| = 1\} \quad (2.9)$$

is a level set of ω . If $J_f \neq 0$, then $\mathcal{C} \setminus \mathcal{M}$ consists of analytic curves. These intersect in $z \in \mathcal{C} \setminus \mathcal{M}$ if, and only if, $\omega'(z) = 0$. At $z \in \mathcal{C} \setminus \mathcal{M}$ with $\omega'(z) \neq 0$, the equation

$$\omega(\gamma(t)) = e^{it}, \quad t \in I \subseteq \mathbb{R}, \quad (2.10)$$

implicitly defines a local analytic parametrization $z = \gamma(t)$ of $\mathcal{C} \setminus \mathcal{M}$.

Definition 2.2. We call the set of critical values of f , i.e. $f(\mathcal{C})$, the *caustics* or the *set of caustic points*. The caustics induce a partition of $\mathbb{C} \setminus f(\mathcal{C})$, and we call a connected component $A \subseteq \mathbb{C} \setminus f(\mathcal{C})$ with $\partial A \subseteq f(\mathcal{C})$ a *caustic tile*.

The next lemma characterizes a tangent vector to the caustics; see [28, Lem. 2.1] or [21, Lem. 2.3].

Lemma 2.3. *Let f be a harmonic mapping, $z_0 \in \mathcal{C} \setminus \mathcal{M}$ with $\omega'(z_0) \neq 0$, and let $z_0 = \gamma(t_0)$ with the parametrization (2.10). Then $f \circ \gamma$ is a parametrization of a caustic and the corresponding tangent vector at $f(z_0)$ is*

$$\tau(t_0) = \frac{d}{dt}(f \circ \gamma)(t_0) = e^{-it_0/2} \psi(t_0) \quad (2.11)$$

with

$$\psi(t) = 2 \operatorname{Re}(e^{it/2} \partial_z f(\gamma(t)) \gamma'(t)). \quad (2.12)$$

In particular, the rate of change of the argument of the tangent vector is

$$\frac{d}{dt} \arg(\tau(t)) \Big|_{t=t_0} = -\frac{1}{2}, \quad (2.13)$$

at points where $\psi(t_0) \neq 0$, i.e., the curvature of the caustics is constant with respect to the parametrization $f \circ \gamma$. Moreover, ψ has either only finitely many zeros, or is identically zero, in which case $f \circ \gamma$ is constant.

Definition 2.4 ([28, Def. 2.2]). In the notation of Lemma 2.3, we call $f(\gamma(t_0))$ a *fold caustic point* or simply a *fold*, if the tangent $\tau(t_0)$ is non-zero, and a *cuspl*, if ψ has a zero with a sign change at t_0 .

This classification of caustic points is not complete, but sufficient for our needs. Fold points form open arcs of the caustic curves, since ψ is continuous. At a cuspl, the argument of the tangent vector changes by $+\pi$. The cusps and the curvature of the caustics are apparent in Figure 1 (left) below, as well as the four caustic tiles.

2.3 Pre-images under non-degenerate harmonic mappings

The position of $\eta \in \mathbb{C}$ with respect to the caustics affects the number of pre-images of η under f . The following wide class of harmonic mappings was introduced in [28, Def. 3.1].

Definition 2.5. We call a harmonic mapping f *non-degenerate* on $\widehat{\mathbb{C}}$, if

1. f is defined in $\widehat{\mathbb{C}}$, except at finitely many poles $z_1, \dots, z_m \in \widehat{\mathbb{C}}$,
2. at each pole $z_j \in \mathbb{C}$ of f , the decomposition (2.2) of f has the form

$$f(z) = \sum_{k=-n}^{\infty} a_k(z - z_j)^k + \overline{\sum_{k=-n}^{\infty} b_k(z - z_j)^k} + 2A_j \log|z - z_j| \quad (2.14)$$

with $n \geq 1$ and $|a_{-n}| \neq |b_{-n}|$. And if $z_j = \infty$ is a pole of f , then

$$f(z) = \sum_{k=-\infty}^n a_k z^k + \overline{\sum_{k=-\infty}^n b_k z^k} + 2A_j \log|z|, \quad \text{for } |z| > R, \quad (2.15)$$

with $n \geq 1$ and $|a_n| \neq |b_n|$, and $R > 0$,

3. the critical set of f is bounded in \mathbb{C} .

The intensively studied (see references in the introduction) rational harmonic mappings $r(z) - \bar{z}$ and harmonic polynomials $p(z) + \overline{q(z)}$ are non-degenerate if, and only if, $\lim_{z \rightarrow \infty} |r(z)/z| \neq 1$ and $\lim_{z \rightarrow \infty} |p(z)/q(z)| \neq 1$, respectively, since ∞ is the only pole of $p(z)$, $q(z)$, and z .

A non-degenerate harmonic mapping f has a global decomposition (2.3), and

$$\partial_z f(z) = r'(z) + \sum_{j=1}^m \frac{A_j}{z - z_j}, \quad \overline{\partial_z f(z)} = s'(z) + \sum_{j=1}^m \frac{\bar{A}_j}{z - z_j}, \quad (2.16)$$

are rational functions. By item 2., the poles are not accumulation points of the critical set [32, Lem. 2.2, 2.3]. Hence, \mathcal{C} and $f(\mathcal{C})$ are compact sets in

\mathbb{C} . Item 3. implies that $J_f \not\equiv 0$. If $\partial_z f \equiv 0$, then $\overline{\partial_z f} \not\equiv 0$ (since $J_f \not\equiv 0$), and \mathcal{C} consists of the finitely many zeros of the rational function $\overline{\partial_z f}$. If $\partial_z f \not\equiv 0$, then $\omega = \overline{\partial_z f} / \partial_z f$ is rational, \mathcal{M} has only finitely many points, and $\mathcal{C} \setminus \mathcal{M}$ consists of the $\deg(\omega)$ many pre-images of the unit circle under ω . We can parametrize $\mathcal{C} \setminus \mathcal{M}$ with analytic closed curves according to (2.10), such that every $z \in \mathcal{C} \setminus \mathcal{M}$ with $\omega'(z) \neq 0$ belongs exactly to one curve; see [28, pp. 10–11]. We call these curves the *critical curves* of f and denote the set of all of them by crit . The critical curves and their images under f have both finite total length since their parametrization is piecewise C^∞ .

Let $P(f) = n_1 + \dots + n_m$ be the sum of the orders of the poles z_1, \dots, z_m in (2.14) or (2.15). Then $N_\eta(f) = |\{z \in \widehat{\mathbb{C}} : f(z) = \eta\}|$ relates to $P(f)$ and the winding number $n(f \circ \gamma; \eta)$ of the caustics about η as follows.

Theorem 2.6 ([28, Thms. 3.4, 3.7]). *Let f be a non-degenerate harmonic mapping on $\widehat{\mathbb{C}}$. Then, for a point $\eta \in \mathbb{C} \setminus f(\mathcal{C})$, we have*

$$N_\eta(f) = P(f) + 2 \sum_{\gamma \in \text{crit}} n(f \circ \gamma; \eta). \quad (2.17)$$

In particular, the number of pre-images of $\eta \in \mathbb{C} \setminus f(\mathcal{C})$ under f is finite. Moreover, if $\eta_1, \eta_2 \in \mathbb{C} \setminus f(\mathcal{C})$, then

$$N_{\eta_2}(f) = N_{\eta_1}(f) + 2 \sum_{\gamma \in \text{crit}} (n(f \circ \gamma; \eta_2) - n(f \circ \gamma; \eta_1)), \quad (2.18)$$

and we have:

1. *If η_1 and η_2 are in the same caustic tile, then the number of pre-images under f is the same, i.e., $N_{\eta_2}(f) = N_{\eta_1}(f)$.*
2. *If η_1 and η_2 are separated by a single caustic arc $f \circ \gamma$, then the number of pre-images under f changes by two, i.e., $N_{\eta_2}(f) = N_{\eta_1}(f) \pm 2$.*

Example 2.7 ([28, Ex. 3.10]). We study the non-degenerate harmonic mapping

$$f(z) = z^2 + \overline{z^{-1} + (z+1)^{-1}} + 2 \log|z|, \quad (2.19)$$

see Figure 1. By Lemma 2.3, the curvature of a caustic is always negative. Consequently, the winding numbers of the only caustic $f \circ \gamma$ about η_1, η_2 and η_3 are 0, -1 and 1 respectively. By Theorem 2.6 we have

$$\begin{aligned} N_{\eta_1}(f) &= P(f) + 2n(f \circ \gamma; \eta_1) = 4 + 0 = 4, \\ N_{\eta_2}(f) &= N_{\eta_1}(f) + 2(n(f \circ \gamma; \eta_2) - n(f \circ \gamma; \eta_1)) = 4 - 2 = 2, \\ N_{\eta_3}(f) &= N_{\eta_1}(f) + 2(n(f \circ \gamma; \eta_3) - n(f \circ \gamma; \eta_1)) = 4 + 2 = 6, \end{aligned}$$

as we see in Figure 1.

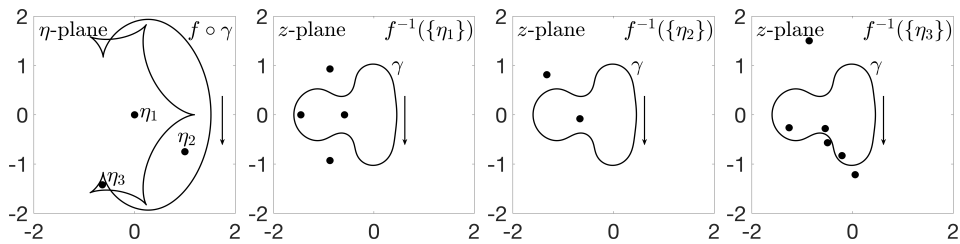


Figure 1: Harmonic mapping (2.19). η -plane: the caustic $f \circ \gamma$ of f and the points η_j . z -plane: pre-images of η_j under f . The arrows indicate the orientation of the critical curve γ and the caustic $f \circ \gamma$.

3 The transport of images method

We compute all zeros of a non-degenerate harmonic mapping by continuation. Recall from the introduction that we successively compute all solutions of $f(z) = \eta_k$ for a sequence η_1, η_2, \dots that tends to zero. During this procedure, the number of solutions may differ, depending on the positions of the points η_k relative to the caustics of f ; see Theorem 2.6. We start by computing all solutions of $f(z) = \eta_1$ for $|\eta_1|$ sufficiently large from the poles of f . Given all solutions of $f(z) = \eta_k$, we determine $\eta_{k+1} \in \mathbb{C}$ and $S_{k+1} \subset \mathbb{C}$ (prediction), such that the following holds: (1) for every solution $z_* \in \mathbb{C}$ of $f(z) = \eta_{k+1}$, there exists a $z_0 \in S_{k+1}$, such that the sequence $(z_j)_{j \in \mathbb{N}}$ of Newton iterates for $f - \eta_{k+1}$ converges to z_* (correction); (2) the number of solutions of $f(z) = \eta_{k+1}$ coincides with the number of elements in S_{k+1} , i.e., S_{k+1} is minimal. When this prediction-correction scheme reaches $\eta_n = 0$, we have computed *all* zeros of f . This leads to the following algorithm.

The transport of images method

1. *Initial phase*: compute all solutions of $f(z) = \eta_1$.
2. *Transport phase*: while $\eta_k \neq 0$ do
 - (a) *Prediction*: choose $\eta_{k+1} \in \mathbb{C}$ and construct a minimal set of initial points S_{k+1} from the solutions of $f(z) = \eta_k$ and from the caustics.
 - (b) *Correction*: apply Newton's method to $f - \eta_{k+1}$ with the set of initial points S_{k+1} to get all solutions of $f(z) = \eta_{k+1}$.

The points $\eta_1, \eta_2, \dots, \eta_n = 0$ conceptually form a path in \mathbb{C} (see Figure 2). From this perspective, the transport of images method discretizes the tracing of the solution curves of $f(z) = \eta(t)$, where the right hand side is a path $\eta : [a, b] \rightarrow \mathbb{C}$. We describe the homotopy curves for a general harmonic mapping in Section 3.4 in full detail.

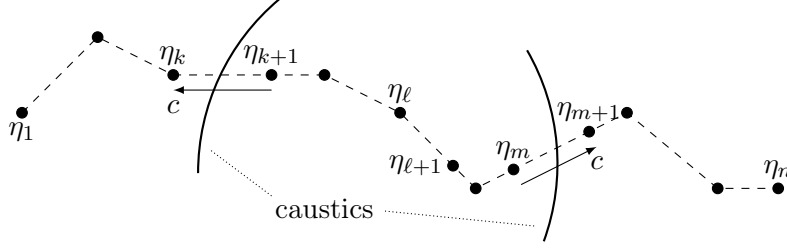


Figure 2: A path from η_1 to η_n with the three kind of steps in the transport of images method: (1) $f(z) = \eta_{k+1}$ has two solutions more than $f(z) = \eta_k$, (2) the number of solutions for η_ℓ and $\eta_{\ell+1}$ coincides, and (3) $f(z) = \eta_{m+1}$ has two solutions less than $f(z) = \eta_m$.

3.1 Newton's method as corrector

For a harmonic mapping $f : \Omega \rightarrow \mathbb{C}$, the *harmonic Newton map* is

$$H_f : \Omega \setminus \mathcal{C} \rightarrow \mathbb{C}, \quad H_f(z) = z - \frac{\overline{h'(z)}f(z) - \overline{g'(z)}f(z)}{|h'(z)|^2 - |g'(z)|^2}, \quad (3.1)$$

where $f = h + \bar{g}$ is a local decomposition (2.1), and the *harmonic Newton iteration* with initial point $z_0 \in \Omega \setminus \mathcal{C}$ is

$$z_k = H_f(z_{k-1}) = H_f^k(z_0), \quad k \geq 1. \quad (3.2)$$

We write, as usual, $H_f^k(z) = H_f(H_f^{k-1}(z))$ for $k \geq 1$ and $H_f^0(z) = z$. The iteration (3.2) is a complex formulation of the classical Newton iteration in \mathbb{R}^2 [29, Sect. 3.1], and hence inherits all properties of Newton's method, e.g., the local quadratic convergence.

To compute solutions of $f(z) = \eta$ with $\eta \in \mathbb{C}$, we apply the iteration (3.2) to $f - \eta$. The limit of the harmonic Newton iteration with initial point z_0 ,

$$H_{f-\eta}^\infty(z_0) = \lim_{k \rightarrow \infty} H_{f-\eta}^k(z_0), \quad (3.3)$$

exists for all z_0 in a neighborhood of a solution $z_* \notin \mathcal{C}$ of $f(z) = \eta$ by the local convergence property of Newton's method. If $z_* = H_{f-\eta}^\infty(z_0)$ holds, we say that z_* *attracts* z_0 under $H_{f-\eta}$, or z_0 is *attracted* by z_* under $H_{f-\eta}$.

Definition 3.1. For a harmonic mapping f , we call a set S a (*minimal*) *prediction set* of $f^{-1}(\{\eta\})$, if every solution of $f(z) = \eta$ attracts exactly one point in S under $H_{f-\eta}$, i.e., if $H_{f-\eta}^\infty(S) = f^{-1}(\{\eta\})$, and $|S| = |f^{-1}(\{\eta\})|$.

For a prediction set S , the map $H_{f-\eta}^\infty$ is a bijection from S to $f^{-1}(\{\eta\})$. In this sense, every point $z_0 \in S$ represents exactly one solution of $f(z) = \eta$. In [31], the point z_0 is called an *approximate zero* of $f - \eta$, if the Newton iterates additionally satisfy $|z_k - z_{k-1}| \leq (\frac{1}{2})^{2^{k-1}-1} |z_1 - z_0|$.

3.2 Initial phase

For non-degenerate harmonic mappings, the initial phase can be realized as follows. For sufficiently large $|\eta|$, all solutions of $f(z) = \eta$ are close to the poles of f , and, in the notation (2.14) or (2.15), there are exactly n solutions close to the pole z_j [28, Thm. 3.6]. We compute these solutions with the harmonic Newton iteration and the initial points from the next theorem. A similar result holds if ∞ is a pole of f ; generalizing [29, Cor. 4.5]. All initial points together give a prediction set of $f^{-1}(\{\eta\})$.

Theorem 3.2. *Let f be harmonic in $D = \{z \in \mathbb{C} : 0 < |z - z_0| < r\}$ with*

$$f(z) = \sum_{k=-n}^{\infty} a_k (z - z_0)^k + \overline{\sum_{k=-n}^{\infty} b_k (z - z_0)^k} + 2A \log|z - z_0|, \quad z \in D,$$

where $n \geq 1$, and $|a_{-n}| \neq |b_{-n}|$. Suppose that $c = \eta - (a_0 + \bar{b}_0) \neq 0$, and let ζ_1, \dots, ζ_n be the n solutions of

$$(\zeta - z_0)^n = \frac{|a_{-n}|^2 - |b_{-n}|^2}{\bar{a}_{-n}c - \bar{b}_{-n}\bar{c}}. \quad (3.4)$$

We then have for sufficiently large $|c|$, i.e., for sufficiently large $|\eta|$:

1. There exist exactly n solutions of $f(z) = \eta$ near z_0 .
2. The set $S = \{\zeta_1, \dots, \zeta_n\}$ is a prediction set for the solutions in 1.

Proof. If $A = 0$, then $f - \eta$ has n distinct zeros near z_0 , which satisfy 2. by [29, Thm. 4.3]. For $A \neq 0$, the proof closely follows the proof of [29, Thm. 4.3], if one replaces h' by $\partial_z f$, and g' by $\overline{\partial_{\bar{z}} f}$. As in the proof of [28, Thm. 3.6], Rouché's theorem (e.g. [27, Thm. 2.3]) implies that $f - \eta$ cannot have more than n zeros in a neighborhood of z_0 . \square

3.3 Transport phase

We analyze the prediction-correction scheme of the transport phase and show that the transport phase can be realized with a finite number of steps. We begin with a single step and investigate how all solutions of $f(z) = \eta_2$ can be determined, given all solutions of $f(z) = \eta_1$. First, we prove that a solution of $f(z) = \eta_1$ that is not in \mathcal{C} , is attracted by a solution of $f(z) = \eta_2$ under the harmonic Newton map $H_{f-\eta_2}$, if $|\eta_2 - \eta_1|$ is small enough.

Lemma 3.3. *Let $f : \Omega \rightarrow \mathbb{C}$ be a harmonic mapping, $z_0 \in \Omega \setminus \mathcal{C}$ and $\eta_1 = f(z_0)$. Then there exist $\varepsilon > 0$ and $\delta > 0$ such that for each $\eta_2 \in D_\varepsilon(\eta_1)$ there exists a unique $z_* \in D_\delta(z_0)$ with $f(z_*) = \eta_2$. Moreover, z_* attracts z_0 under the harmonic Newton map $H_{f-\eta_2}$, i.e., $H_{f-\eta_2}^\infty(z_0) = z_*$.*

Proof. Let $\zeta \in \Omega \setminus \mathcal{C}$ and consider $f - f(\zeta)$. The Newton-Kantorovich theorem yields a radius $\rho(\zeta) > 0$ so that ζ attracts all points in $D_{\rho(\zeta)}(\zeta)$ under the harmonic Newton map of $f - f(\zeta)$; see [29, Thm. 2.2, Sect. 4] and references therein. (The basin of attraction of ζ might be larger.) Note that ρ depends continuously on ζ .

There exist open neighborhoods $U \subseteq \Omega \setminus \mathcal{C}$ of z_0 and V of η_1 such that $f : U \rightarrow V$ is a diffeomorphism (inverse function theorem). Let $r > 0$ with $K = \overline{D_r(z_0)} \subseteq U$, and let $m = \min_{z \in K} \rho(z)$. Then $m > 0$ since K is compact and ρ is continuous with $\rho(z) > 0$ for $z \in U$. Let $0 < \delta \leq \min\{r, m\}$. Then $z_* \in D_\delta(z_0)$ satisfies $|z_* - z_0| < \delta \leq m \leq \rho(z_*)$, hence $H_{f-f(z_*)}^\infty(z_0) = z_*$. Finally, there exists $\varepsilon > 0$ with $D_\varepsilon(\eta_1) \subseteq f(D_\delta(z_0))$. \square

By Theorem 2.6, two points in a same caustic tile have the same number of pre-images. Moreover, $\eta \in \mathbb{C} \setminus f(\mathcal{C})$ has only finitely many pre-images, and these are in $\widehat{\mathbb{C}} \setminus \mathcal{C}$. Thus, we can apply Lemma 3.3 to all solutions simultaneously to obtain the next theorem.

Theorem 3.4. *Let f be a non-degenerate harmonic mapping on $\widehat{\mathbb{C}}$, and let $\eta_1 \in \mathbb{C} \setminus f(\mathcal{C})$. Then there exists an $\varepsilon > 0$, such that $S = f^{-1}(\{\eta_1\})$ is a prediction set of $f^{-1}(\{\eta_2\})$ for all $\eta_2 \in D_\varepsilon(\eta_1) \subseteq \mathbb{C} \setminus f(\mathcal{C})$.*

By Theorem 2.6, the number of pre-images of η_1, η_2 differs by 2, if η_1, η_2 are in adjacent caustic tiles separated by a single caustic arc. The two additional solutions can be computed with the next theorem, provided that the step from η_1 to η_2 crosses the caustics in a specific direction.

Theorem 3.5 ([28, Thm. 4.2]). *Let $f : \Omega \rightarrow \mathbb{C}$ be a harmonic mapping and $z_0 \in \mathcal{C} \setminus \mathcal{M}$, such that $\eta = f(z_0)$ is a fold caustic point. Moreover, let*

$$f(z) = \sum_{k=0}^{\infty} a_k (z - z_0)^k + \overline{\sum_{k=0}^{\infty} b_k (z - z_0)^k} \quad \text{and} \quad c = - \left(\frac{a_2 \bar{b}_1}{a_1} + \frac{\bar{b}_2 a_1}{\bar{b}_1} \right). \quad (3.5)$$

Then, for each sufficiently small $\varepsilon > 0$, there exists a $\delta > 0$, such that for all $0 < t < \delta$:

1. $f(z) = \eta - tc$ has no solution in $D_\varepsilon(z_0)$,
2. $f(z) = \eta$ has exactly one solution in $D_\varepsilon(z_0)$,
3. $f(z) = \eta + tc$ has exactly two solutions in $D_\varepsilon(z_0)$.

Moreover, each solution in 3. attracts one of the points

$$z_\pm = z_0 \pm i \sqrt{t \bar{b}_1 / a_1}, \quad (3.6)$$

under the harmonic Newton map $H_{f-(\eta+tc)}$, if $t > 0$ is sufficiently small.

Note that f is *light* (i.e., $f^{-1}(\{\eta\})$ is either totally disconnected or empty for all $\eta \in \mathbb{C}$) in a neighborhood of z_0 if $f(z_0)$ is a fold [28, Rem. 2.3], hence we omit this assumption from [29, Thm. 4.2]. We emphasize that c is not necessarily a normal vector to the caustics.

With Theorem 3.5, we construct a prediction set of $f^{-1}(\{\eta_2\})$, when the step from η_1 to η_2 crosses a caustic at a *simple fold* η , i.e., $|f^{-1}(\{\eta\}) \cap \mathcal{C}| = 1$.

Theorem 3.6. *Let f be a non-degenerate harmonic mapping on $\widehat{\mathbb{C}}$. Let $\eta_1, \eta_2 \in \mathbb{C} \setminus f(\mathcal{C})$, such that there exists exactly one simple fold η and no other caustic point on the line segment from η_1 to η_2 , and such that $\arg(\eta_2 - \eta_1) = \arg(\pm c)$, where c is defined as in Theorem 3.5. Then, for small enough $|\eta_2 - \eta_1|$,*

$$S = \begin{cases} f^{-1}(\{\eta_1\}) \cup \{z_{\pm}\}, & \text{if } \arg(\eta_2 - \eta_1) = \arg(+c), \\ f^{-1}(\{\eta_1\}) \setminus H_{f^{-\eta_1}}^{\infty}(\{z_{\pm}\}), & \text{if } \arg(\eta_2 - \eta_1) = \arg(-c), \end{cases} \quad (3.7)$$

is a prediction set of $f^{-1}(\{\eta_2\})$, with z_{\pm} from (3.6).

Proof. Let $\eta = f(z_0)$ be the unique simple fold on the line segment between η_1 and η_2 . The step from η_1 to η_2 produces either two additional or two fewer solutions in a neighborhood of z_0 , depending on c ; see Theorem 3.5. The global number of solutions changes accordingly; see Theorem 2.6.

In case of two additional solutions, i.e., if $\arg(\eta_2 - \eta_1) = \arg(+c)$, the set S contains the solutions of $f(z) = \eta_1$, and the points z_{\pm} , hence $|S| = |f^{-1}(\{\eta_2\})|$ for sufficiently small $|\eta_2 - \eta_1|$. Let $t_1, t_2 > 0$, such that $\eta_1 = \eta - t_1 c$ and $\eta_2 = \eta + t_2 c$. In particular we have $t_j \leq |(\eta_2 - \eta_1)/c|$. In the disk $D_{\varepsilon}(z_0)$ from Theorem 3.5, $f(z) = \eta_1$ has no solution, and $f(z) = \eta_2$ has exactly two solutions which attract z_+ and z_- , respectively, if $|\eta_2 - \eta_1|$ and hence t_2 are small enough. Since η_1 is not a caustic point, all solutions of $f(z) = \eta_1$ are not in \mathcal{C} . Hence, every solution of $f(z) = \eta_2$ outside $D_{\varepsilon}(z_0)$ attracts exactly one solution of $f(z) = \eta_1$ by Lemma 3.3, when $|\eta_2 - \eta_1|$ is sufficiently small. Together, S is a prediction set of $f^{-1}(\{\eta_2\})$.

In case of two fewer solutions, i.e., if $\arg(\eta_2 - \eta_1) = \arg(-c)$, we remove two points from $f^{-1}(\{\eta_1\})$ to obtain a prediction set. To determine these points, we consider the reversed step from η_2 to η_1 . This step gives the two additional solutions $H_{f^{-\eta_1}}^{\infty}(z_{\pm})$, which we remove from $f^{-1}(\{\eta_1\})$ to get S . Each solution of $f(z) = \eta_2$ attracts exactly one point in S , as above. \square

Remark 3.7. Let $\eta \in f(\mathcal{C})$ be a (multiple) fold caustic point, i.e., for each $z_j \in \{z_1, \dots, z_m\} = f^{-1}(\{\eta\}) \cap \mathcal{C}$ the tangent τ_j from (2.11) is non-zero. Then, for every $d \in \mathbb{C}$ with $\text{Im}(\bar{\tau}_j d) \neq 0$ for all $j = 1, \dots, m$, the effect of Theorem 3.5 happens at all points z_1, \dots, z_m simultaneously. By [28, Rem. 4.3], $f(z) = \eta + td$ has 2 solutions in $D_{\varepsilon}(z_j)$ and $f(z) = \eta - td$ has no solutions in $D_{\varepsilon}(z_j)$, if $\text{Im}(\bar{\tau}_j d) > 0$ and $t > 0$ is sufficiently small. If $\text{Im}(\bar{\tau}_j d) < 0$, then $f(z) = \eta \pm td$ swap their roles. However, it is not

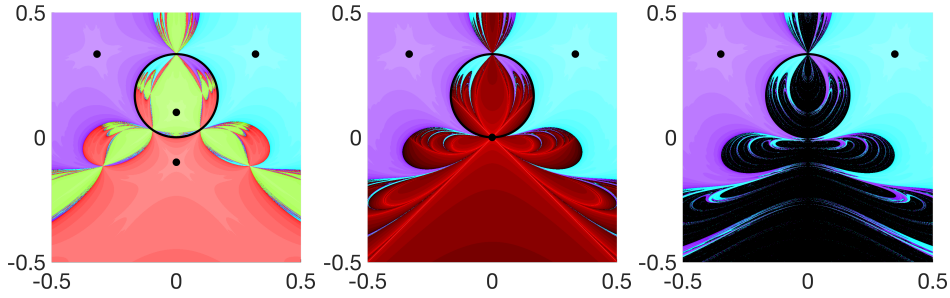


Figure 3: Solutions (black dots) of $f(z) = z + 2iz + \overline{z + iz^2} = tc$ with basins of attraction, with $z_0 = 0$, $c = -i$ and from left to right $t = 0.01$, $t = 0$, $t = -0.01$; see Remark 3.8. The black circle is the critical set of f .

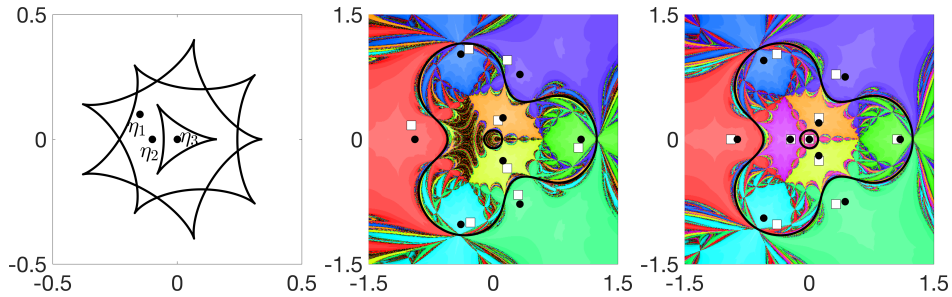


Figure 4: Illustration of Theorems 3.4 and 3.6 for $f(z) = z - \overline{z^2 / (z^3 - 0.6^3)}$ (see (5.2) below). Left: caustics and η_1 , η_2 , η_3 . Middle: prediction set $S = f^{-1}(\{\eta_1\})$ (white squares) of $f^{-1}(\{\eta_2\})$ (black dots). Right: prediction set $S = f^{-1}(\{\eta_2\}) \cup \{z_{\pm}\}$ (white squares) of $f^{-1}(\{\eta_3\})$ (black dots).

guaranteed that the additional solutions attract the points $z_{\pm}(z_j)$ if $\arg(d) \neq \arg(\pm c(z_j))$, with z_{\pm} , c from Theorem 3.5.

Remark 3.8. The basins of attraction of the two solutions of $f(z) = \eta + tc$ in $D_{\varepsilon}(z_0)$ ($t > 0$) merge ($t = 0$) and disappear ($t < 0$) with the solutions. This is illustrated in Figure 3. Points which are attracted by the same solution have the same color. The darker the shading, the more iterations are needed until (numerical) convergence. Points where the iteration does not converge (numerically) are colored in black. This highlights why it is important to remove the two points $H_{f-\eta_1}^{\infty}(z_{\pm})$ from $f^{-1}(\{\eta_1\})$ in (3.7) for practical computations.

We illustrate Theorems 3.4 and 3.6 in Figure 4. First, consider the step from η_1 to η_2 and the dynamics of $H_{f-\eta_2}$ (middle plot). Every basin of attraction contains exactly one element of $S = f^{-1}(\{\eta_1\})$, i.e., S is a prediction set of $f^{-1}(\{\eta_2\})$. Some elements in S are close to the boundary of the respective basins, such that S may not be a prediction set of $f^{-1}(\{\eta_2\})$.

for a slightly different η_2 . Since the step from η_2 to η_3 crosses a caustic, the number of solutions of $f(z) = \eta_2$ and $f(z) = \eta_3$ differ. According to Theorem 3.6, $S = f^{-1}(\{\eta_2\}) \cup \{z_{\pm}\}$ with the points z_{\pm} from (3.6) is a prediction set of $f^{-1}(\{\eta_3\})$, shown in the right plot.

Theorems 3.2, 3.4 and 3.6 establish the transport of images method, if the points η_k are chosen properly. This motivates the next definition.

Definition 3.9. Let f be a non-degenerate harmonic mapping on $\widehat{\mathbb{C}}$. We call $(\eta_1, \dots, \eta_n) \in \mathbb{C}^n$ a *transport path* from η_1 to η_n , if for each $k = 1, \dots, n-1$ either $f^{-1}(\{\eta_k\})$ or S in (3.7) is a prediction set of $f^{-1}(\{\eta_{k+1}\})$.

Along a transport path, all solutions of $f(z) = \eta_{k+1}$ can be computed from the solutions of $f(z) = \eta_k$. Next, we show the existence of such paths. Here, we call η a multiple caustic point, if $|f^{-1}(\{\eta\}) \cap \mathcal{C}| > 1$.

Theorem 3.10. *Let f be a non-degenerate harmonic mapping on $\widehat{\mathbb{C}}$ without non-isolated multiple caustic points, and let $\eta_s, \eta_e \in \mathbb{C} \setminus f(\mathcal{C})$. Then there exists a transport path from η_s to η_e .*

Proof. We show that there exists a polygonal path from η_s to η_e , which intersects the caustics only at a finite number of simple fold points. Then this path is refined if necessary.

Let R be the complex plane \mathbb{C} without caustic points that are not simple fold points, which is \mathbb{C} minus a set of isolated points, and hence a region (open and connected). Since f is non-degenerate, $\partial_z f$, $\overline{\partial_z f}$, and ω are (analytic) rational functions, see (2.16). This has several implications. The sets \mathcal{M} from (2.7) and $f(\mathcal{M})$ are finite. The set $\mathcal{C} \setminus \mathcal{M}$ consists of $\deg(\omega)$ many pre-images of the unit circle under ω . There are at most finitely many critical points z_0 of f with $\omega'(z_0) = 0$, hence the number of caustic points where the tangent (2.11) does not exist is finite. The number of caustic points where the tangent exists and is zero is finite by Lemma 2.3 (on each of the $\deg(\omega)$ many pre-images of the unit circle, there are at most finitely many points with $\tau = 0$, or the whole arc is mapped onto a single point). By assumption, multiple caustic points are isolated.

Next, we prove that there exists a rectifiable path from η_s and η_e in R with only finitely many caustic points (simple folds) on it. Since $\eta_s, \eta_e \notin f(\mathcal{C})$ and the caustics are compact, there exists $\delta > 0$ such that $D_\delta(\eta_s), D_\delta(\eta_e)$ contain no caustic points. We consider the increasing sequence of regions $U_k \subseteq R$ whose points are ‘‘at most k caustic crossings distant’’ from η_s , constructed as follows. Let U_0 be the component (maximal open and connected set) of $R \setminus f(\mathcal{C})$ with $\eta_s \in U_0$. Suppose that $U_k \subseteq R$ has been constructed. Let U_{k+1} be the component of $R \setminus (f(\mathcal{C}) \setminus (\partial U_0 \cup \dots \cup \partial U_k))$ with $\eta_s \in U_{k+1}$. If $\eta_e \in U_k$, there exists a rectifiable path from η_s to η_e in R intersecting $\partial U_0, \dots, \partial U_{k-1}$, and hence has k caustic crossings. If $\eta_e \notin U_k$, then the boundary of U_k in R , which consists of caustic arcs, has length at

least $2\pi\delta$, since then $D_\delta(\eta_s) \subseteq U_k$ and $D_\delta(\eta_e) \subseteq R \setminus U_k$. Let $m = \lceil \frac{L}{2\pi\delta} \rceil$, where $L < \infty$ is the total length of the caustics (see the discussion below Definition 2.5). Then $\eta_e \in U_m$, and there exists a rectifiable path from η_s to η_e , with at most m caustic points.

By manipulations in an arbitrary small neighborhood around this path in R , we obtain a polygonal path $P = (\eta_1, \dots, \eta_n)$ with $\eta_1 = \eta_s$ and $\eta_n = \eta_e$, such that: (1) $\eta_1, \dots, \eta_n \in \mathbb{C} \setminus f(\mathcal{C})$, (2) each line segment $[\eta_k, \eta_{k+1}]$ contains at most one caustic point, (3) if the line segment $[\eta_k, \eta_{k+1}]$ contains a caustic point, then $\arg(\eta_{k+1} - \eta_k) = \arg(\pm c)$, with c as in Theorem 3.5.

We refine this path to get a transport path. First, we consider the line segments $[\eta_k, \eta_{k+1}]$, which contain a caustic point η , but where S in (3.7) is not a prediction set of $f^{-1}(\{\eta_{k+1}\})$. We add two points from $[\eta_k, \eta_{k+1}] \setminus f(\mathcal{C})$ sufficiently close to η , such that Theorem 3.6 applies to these points. Denote the refined path for simplicity again by $P = (\eta_1, \dots, \eta_n)$. Next, we refine the line segments $E = [\eta_k, \eta_{k+1}]$ without caustic points. For all $\eta \in E$ there exists an $\varepsilon(\eta) > 0$, such that $f^{-1}(\{\eta\})$ is a prediction set of $f^{-1}(\{\xi\})$ for all $\xi \in D_{\varepsilon(\eta)}(\eta)$ by Theorem 3.4. The family $(D_{\varepsilon(\eta)}(\eta))_{\eta \in E}$ is an open covering of the compact set E . Hence, there exists a finite sub-covering $(D_{\varepsilon(\kappa_j)}(\kappa_j))_{j=1, \dots, \ell}$ with $\kappa_1 = \eta_k$ and $\kappa_\ell = \eta_{k+1}$, which gives a partition of E , where $f^{-1}(\{\kappa_j\})$ is a prediction set of $f^{-1}(\{\kappa_{j+1}\})$ for $j = 1, \dots, \ell - 1$. Refining all line segments without caustic points yields a transport path. \square

Note that non-degenerate harmonic mappings can actually have non-isolated multiple caustic points.

Example 3.11. The harmonic mapping $f(z) = \frac{1}{2}(z^2 - 1)^2 + \overline{z^2 - 1}$ from [28, Ex. 5.1] is non-degenerate, and maps its critical arcs $\gamma_\pm : [-\pi, \pi] \rightarrow \mathcal{C}$, $\gamma_\pm(t) = \pm\sqrt{1 + e^{-it}}$, onto the same caustic arc.

We close this section by noting the correctness of the transport of images method, provided 0 is not a caustic point of f .

Corollary 3.12. *Let f be a non-degenerate harmonic mapping on $\widehat{\mathbb{C}}$ without non-isolated multiple caustic points, such that 0 is not a caustic point. Then there exists a point $\eta_1 \in \mathbb{C} \setminus f(\mathcal{C})$, such that Theorem 3.2 applies to all poles of f , and there exists a transport path from η_1 to 0.*

Proof. Theorem 3.2 applies to all poles for all $\eta_1 \in \mathbb{C}$ with large enough $|\eta_1|$. Since $f(\mathcal{C})$ is compact, η_1 can be chosen in $\mathbb{C} \setminus f(\mathcal{C})$. Then there exists a transport path from η_1 to 0 by Theorem 3.10. \square

3.4 Analysis of the homotopy curves

We now consider the continuous problem behind our (discrete) computation and describe the homotopy curves in the transport of images method, i.e., how the solution set of $f(z) = \eta(t)$ varies with t , where $f : \Omega \rightarrow \mathbb{C}$ is a

harmonic mapping and $\eta : [a, b] \rightarrow \mathbb{C}$, $t \mapsto \eta(t)$, is a (continuous) path. We analyze the solution set locally with results from [21, 29, 28]. Combining the local results gives the global picture. We distinguish the cases (1) $z_0 \in \Omega \setminus \mathcal{C}$, (2) $z_0 \in \mathcal{M}$ and (3) $z_0 \in \mathcal{C} \setminus \mathcal{M}$.

(1) Let $z_0 \in \Omega \setminus \mathcal{C}$, i.e., the Jacobian of f is non-zero at z_0 . By the inverse function theorem, there exists $\varepsilon > 0$ and an open set $V \subseteq \mathbb{C}$ such that $f : D_\varepsilon(z_0) \rightarrow V$ is a diffeomorphism. A curve $\eta(t)$ in V has a unique pre-image curve $z(t) = f^{-1}(\eta(t))$. In particular, the homotopy curves can intersect only at critical points.

(2) Let $z_0 \in \mathcal{M}$ from (2.7). Then f has the form

$$f(z) = a_0 + \sum_{k=n}^{\infty} a_k (z - z_0)^k + b_0 + \overline{\sum_{k=n}^{\infty} b_k (z - z_0)^k}$$

with $n \geq 2$ and $|a_n| \neq |b_n|$. If $\eta(t)$ passes through $f(z_0)$, then exactly n homotopy curves intersect at z_0 with equispaced angles, since $f(z) = \eta(t)$ is locally to leading order $f(z_0) + a_n(z - z_0)^n + \overline{b_n(z - z_0)^n} = \eta(t)$, which has the unique solution

$$(z - z_0)^n = \frac{\overline{a_n}(\eta(t) - f(z_0)) - \overline{b_n}(\eta(t) - f(z_0))}{|a_n|^2 - |b_n|^2},$$

see [29, Lem. 4.2].

(3) For $z_0 \in \mathcal{C} \setminus \mathcal{M}$, the situation is more involved. By [21, Thm. 2.1], a harmonic mapping is either (a) light, (b) has zero Jacobian, or (c) is constant on some arc of $\mathcal{C} \setminus \mathcal{M}$. We discuss all three cases.

(3a) Let f be a light harmonic mapping. Essentially, the behavior of the homotopy curves at z_0 depends on the tangent to the caustics at $f(z_0)$ and hence on ψ from (2.12). Let $z_0 \in \mathcal{C} \setminus \mathcal{M}$. Then z_0 is a zero of order $\ell \geq 0$ of $\partial_z f$ (and of $\partial_{\bar{z}} f$). First, let $\omega'(z_0) \neq 0$, so that $z_0 = \gamma(t_0)$ is a point on a critical curve that is not a self-intersection point of the critical curves.

1. If $\psi(t_0)$ is non-zero ($f(z_0)$ is a fold caustic point and $\ell = 0$), then z_0 is a turning point of the homotopy curves, i.e., two curves start or end at z_0 when $\eta(t)$ crosses the caustics at $f(z_0)$. This follows from Theorem 3.5 or [21, Thm. 5.1], and is illustrated in [28, Fig. 5].
2. More generally, if ψ does not change sign at t_0 , then [21, Thm. 5.1] implies that ℓ homotopy curves intersect at z_0 and two homotopy curves start or end at z_0 , when $\eta(t)$ crosses the caustics at $f(z_0)$. Hence, z_0 is a turning point and, if $\ell > 0$, a bifurcation point of the homotopy curves.
3. If ψ changes sign at t_0 (i.e., $f(z_0)$ is a cusp), then by [21, Thm. 5.1] z_0 is a bifurcation point where $\ell + 1$ homotopy curves intersect and two homotopy curves start or end, when $\eta(t)$ crosses the caustics at $f(z_0)$.

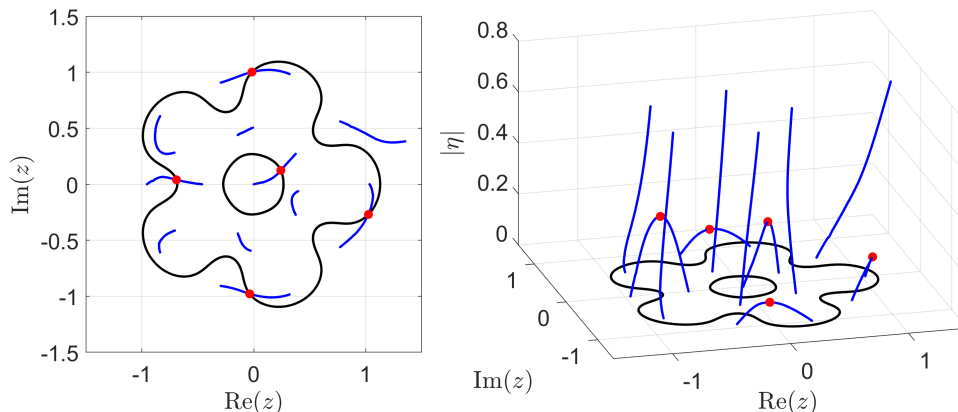


Figure 5: Computed homotopy curves (blue) with turning points (red dots) in Example 3.13, and critical set of f (black).

For $\omega'(z_0) = 0$, there is only an upper bound on the local valence of f at z_0 [21, Sect. 6], and hence on the number of homotopy curves, which also depends on the caustic tiles bordering $f(z_0)$ that are traversed by $\eta(t)$.

Example 3.13. The harmonic mapping (5.2) below is light and non-degenerate. For $n = 5$ and $r = 0.6$, Figure 5 shows the computed homotopy curves when $\eta = \eta(t)$ parametrizes the segment from $0.6699 + 0.1795i$ to 0 , which intersects the caustics of f only at simple fold points. Along this path, each caustic crossing produces two additional solutions. The corresponding turning points of the homotopy curves are marked with red circles. Figure 5 shows the solutions $z(t)$ of $f(z) = \eta(t)$ in the z -plane (left) and over the z -plane at height $|\eta(t)|$ (right).

(3b) Let f be a harmonic mapping with $J_f \equiv 0$, i.e., $\mathcal{C} = \Omega$. Then $f(z) = a \operatorname{Re}(h(z)) + b$ with $a, b \in \mathbb{C}$, $a \neq 0$, and an analytic function h ; see [21, Lem. 2.1] or [23, Lem. 4.7]. (If Ω is not simply connected, h may be multi-valued, but $\operatorname{Re}(h)$ is single-valued.) Then $f(\Omega) \subseteq \{at + b : t \in \mathbb{R}\}$, and $f(z) = \eta$ if, and only if, $\operatorname{Re}(h(z)) = (\eta - b)/a$. Since h is analytic, it is either constant or has the open mapping property, which shows that the solution set of $f(z) = \eta$ is either empty, Ω , or a union of curves. Along a path $\eta(t)$ crossing the caustics of f , the solutions do not form curves depending on t .

Example 3.14. The Jacobian of $f(z) = z + \bar{z}$, vanishes identically. Clearly, $f(z) = \eta \in \mathbb{C} \setminus \mathbb{R}$ has no solution, while $f(z) = \eta \in \mathbb{R}$ is solved by all z with $\operatorname{Re}(z) = \eta/2$.

(3c) Let f be a harmonic mapping that is constant on some arc Γ of $\mathcal{C} \setminus \mathcal{M}$, and $z_0 \in \Gamma$. Then f maps Γ onto the single point $f(z_0)$. For $\eta(t)$ not equal to $f(z_0)$ (or any similar point), the homotopy curves are as for light harmonic mappings. However, when $\eta(t) = f(z_0)$, the solution set also contains all points of Γ , and the solutions do not form curves depending on t .

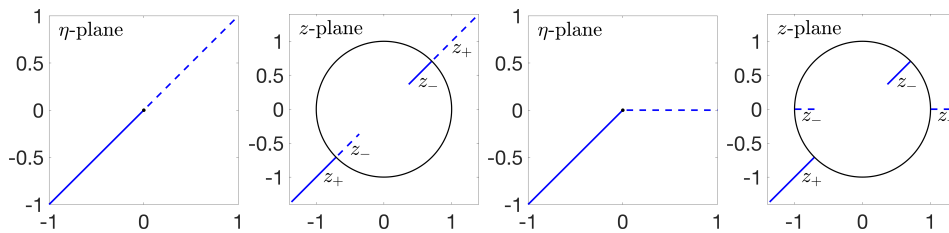


Figure 6: Homotopy curves of $f(z) = z - 1/\bar{z}$ for two paths $\eta(t)$ (panels 1 and 3), divided in a solid and dashed blue part, and corresponding pre-images (panels 2 and 4); see Example 3.15. The black circle is $\mathcal{C} = f^{-1}(\{0\})$.

Example 3.15. The non-degenerate harmonic mapping $f(z) = z - 1/\bar{z}$ is not light since $f^{-1}(\{0\}) = \{z \in \mathbb{C} : |z| = 1\} = \mathcal{C}$. Let $\eta \in \mathbb{C} \setminus \{0\}$. Then $f(z) = \eta$ has the two solutions

$$z_{\pm}(\eta) = \frac{1 \pm \sqrt{1 + 4|\eta|^{-2}}}{2} \eta$$

which satisfy $|z_+(\eta)| > 1$ and $|z_-(\eta)| < 1$, and $|z_{\pm}(\eta)| \rightarrow 1$ when $\eta \rightarrow 0$. Figure 6 shows a path $\eta(t)$ crossing the origin (panel 1) and the corresponding homotopy curves (panel 2). When $\eta(t) = 0$, the two solutions are replaced by all points on the unit circle. Panels 3 and 4 show a similar example with a non-smooth path $\eta(t)$, which leads to homotopy curves exiting \mathcal{C} at different points.

The analysis of the homotopy curves also confirms that Definition 3.9 of a transport path is reasonable. The points η_k are in $\mathbb{C} \setminus f(\mathcal{C})$ to avoid (i) a zero Jacobian at one of the pre-images of η_k , and (ii) potentially infinitely many solutions. Moreover, to avoid bifurcation points of the homotopy curves, transport paths cross the caustics only at fold points, which can be handled by Theorem 3.5.

4 Implementation

A Matlab implementation of our method is freely available at

<https://github.com/transportofimages/>

This toolbox contains routines to compute the zeros of non-degenerate harmonic mappings, and the critical curves and caustics. Moreover, it contains m-files to reproduce all examples in Section 5. We briefly describe two key aspects of our implementation.

4.1 Computation of the caustics

The transport of images methods bases essentially upon the correct handling of caustic crossings. To compute the caustics, we first compute the critical curves. Critical points $z \in \mathcal{C} \setminus \mathcal{M}$ satisfy $\omega(z) = e^{it}$ with $t \in [0, 2\pi[$; see (2.9). Since ω is rational for non-degenerate harmonic mappings, $\omega(z) = e^{it}$ is equivalent to a polynomial equation with $\deg(\omega)$ many solutions. We first solve $\omega(z) = 1$ via the polynomial equation. Then, for $0 = t_1 < t_2 < \dots < t_k < 2\pi$, we successively solve $\omega(z) = e^{it_{j+1}}$ with Newton's method (with initial points $\omega^{-1}(\{e^{it_j}\})$). If successful, this procedure gives $\deg(\omega)$ many (discretized) critical arcs, parametrized according to (2.10). Gluing them together yields the critical curves. Finally, the image under f of the critical curves is a discretization of the caustics of f .

4.2 Construction of transport paths

We construct a transport path to 0 along $R_\theta = \{re^{i\theta} : r > 0\}$, $\theta \in [0, 2\pi[$. Beneficially, the intersection points of the caustic and the ray R_θ can be read off from the argument of the caustic points. Also, as discussed in Remark 3.7, crossing the caustics in a specific direction is not essential, as long as the crossing direction is not tangential to the caustics. For brevity we still call $(\eta_1, \dots, \eta_n) \in \mathbb{C}^n$ a transport path, if $f^{-1}(\{\eta_k\})$ or S in (3.7) is a prediction set of $f^{-1}(\{\eta_{k+1}\})$, even if the step from η_k to η_{k+1} is not in the direction c in Theorem 3.6, i.e., even if $\arg(\eta_{k+1} - \eta_k) \neq \arg(\pm c)$. Determining a suitable angle $\theta \in [0, 2\pi[$ for R_θ can be challenging. In particular, the transport phase (along R_θ) may fail, when too small step sizes are required, or when R_θ is tangential or almost tangential to the caustics, or when R_θ intersects the caustic at or near cusps or other non-fold points. To overcome this difficulty we choose the angle $\theta \in [0, 2\pi[$ at random (e.g., uniformly distributed). If the transport phase with θ is not successful, we restart with a new random angle.

We construct a transport path to 0 along R_θ as follows:

(1) Set $\eta_1 = 2e^{i\theta} \max_{z \in \mathcal{C}} |f(z)|$. If Theorem 3.2 with η_1 does not apply to all poles of f , e.g., two distinct points ζ_j and ζ_ℓ are attracted by the same solution of $f(z) = \eta_1$, we increase $|\eta_1|$ and proceed. Eventually $|\eta_1|$ is large enough and Theorem 3.2 applies to all poles of f simultaneously.

(2) Let $\{\xi_1, \dots, \xi_\ell\} = f(\mathcal{C}) \cap R_\theta$ with $|\xi_1| > \dots > |\xi_\ell| > 0$. We compute these intersection points from the discretized caustics with bisection. For each ξ_k , let $\eta_{2k}, \eta_{2k+1} \in R_\theta$ with equal distance to ξ_k , and such that $|\eta_1| > |\eta_2| > \dots > |\eta_{2\ell+1}| > 0$. Then $P = (\eta_1, \eta_2, \dots, \eta_{2\ell+1}, 0)$ is a potential transport path.

(3) We refine P recursively with the following divide-and-conquer scheme to obtain a transport path.

(3a) If the step from η_j to η_{j+1} , where the line segment $[\eta_j, \eta_{j+1}]$ does

not intersect the caustic, is unsuccessful, i.e., if $f^{-1}(\{\eta_j\})$ is not a prediction set of $f^{-1}(\{\eta_{j+1}\})$, we divide the step from η_j to η_{j+1} into two substeps by inserting $\eta' = (\eta_j + \eta_{j+1})/2$ into P .

(3b) If the step from η_j to η_{j+1} , where the line segment $[\eta_j, \eta_{j+1}]$ intersects the caustic, is unsuccessful, i.e., if S in (3.7) is not a prediction set of $f^{-1}(\{\eta_{j+1}\})$, we divide the step from η_j to η_{j+1} into three substeps by inserting $\eta'_1 = (3\eta_j + \eta_{j+1})/4$ and $\eta'_2 = (\eta_j + 3\eta_{j+1})/4$ into P .

(4) We proceed dividing the steps in (3a) and (3b) until P is a transport path, or until we reached a prescribed recursion depth. In the latter case we restart with a new random angle θ in (1).

5 Numerical examples

In order to verify the numerical results, we test our method on the following functions, for which the number of zeros is known analytically:

1. Wilmschurst's harmonic polynomial

$$f(z) = (z - 1)^n + z^n + \overline{i(z - 1)^n - iz^n}, \quad n \geq 1, \quad (5.1)$$

is non-degenerate and has exactly n^2 zeros. This is the maximum number of zeros of a harmonic polynomial $f(z) = p(z) + \overline{q(z)}$ with $\deg(p) = n$ and $\deg(q) < n$; see [35].

2. The rational harmonic mapping of Mao, Petters and Witt [22],

$$f(z) = z - \overline{\left(\frac{z^{n-1}}{z^n - \rho^n}\right)}, \quad n \geq 3, \quad \rho > 0, \quad (5.2)$$

is non-degenerate and has exactly $3n + 1$ zeros for $\rho < \rho_c$, $2n + 1$ zeros for $\rho = \rho_c$, and $n + 1$ zeros for $\rho > \rho_c$, where

$$\rho_c = \left(\frac{n-2}{n}\right)^{\frac{1}{2}} \left(\frac{2}{n-2}\right)^{\frac{1}{n}},$$

see [19, Prop. 2.1].

3. Rhie's rational harmonic mapping

$$f(z) = z - \overline{\left((1 - \varepsilon)\frac{z^{n-1}}{z^n - \rho^n} + \frac{\varepsilon}{z}\right)}, \quad n \geq 3, \quad \rho, \varepsilon > 0, \quad (5.3)$$

is non-degenerate and has exactly $5n$ zeros if $\rho < \rho_c$ (as above) and if $\varepsilon < \varepsilon^*$, where ε^* depends on n and ρ ; see [19, Thm. 2.2] for details. This is the maximum number of zeros of a harmonic mapping $f(z) = z - \overline{r(z)}$ with a rational function r of degree $n + 1 \geq 2$; see [13, Thm. 1].

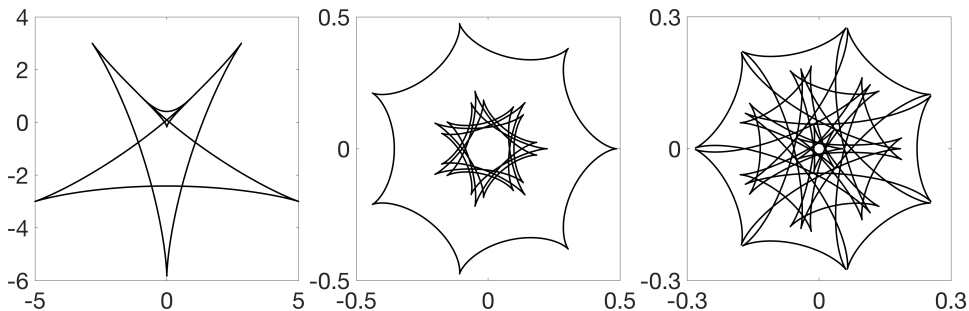


Figure 7: Caustics of harmonic mappings: (5.1) with $n = 3$ (left), (5.2) with $n = 7$ and $\rho = 0.7$ (middle), (5.3) with $n = 7$, $\rho = 0.7$ and $\varepsilon = 0.1$ (right).

Function	zeros	max. res.	N.iter.	steps	ref.
(2.19)	4	6.6613e-16	237	8	2
(5.1), $n = 3$	9	1.7764e-15	291	8	1
(5.2), $n = 7$, $\rho = 0.7$	22	8.9509e-16	1646	19	4
(5.3), $n = 7$, $\rho = 0.7$, $\varepsilon = 0.1$	35	7.8505e-16	3851	40	9

Table 1: Applying the transport of images method: maximal residual (max. res.), number of harmonic Newton iterations (N.iter.), number of transport steps, and number of step refinements (ref.).

These functions should be challenging for the transport of images method, since they have a large number of zeros and very nested caustics; see Figure 7. In gravitational lensing, the functions (5.2), (5.3) and their zeros are of interest; see [19].

The following examples have been performed with our implementation in Matlab R2019b on an i7-7700 4×3.60 GHz CPU with 16 GB RAM.

In our first example, we compute the zeros of (5.1), (5.2), (5.3), and of the transcendental harmonic mapping (2.19) with the transport of images method. Here, we fix the angle $\theta = \pi/50$ in the construction of the transport path (see Section 4.2). The results are displayed in Table 1. We make the following two main observations: (1) In each case, the computed results are very accurate, as shown by the residual $|f(z_j)|$ at the computed zeros which is in the order of the machine precision. Table 1 shows the maximal residual over all computed zeros for the respective functions. (2) Moreover, the transport of images method finishes with the correct number of zeros for each function, in particular for the transcendental harmonic mapping (2.19). The logarithmic term makes a symbolic computation of the zeros difficult, e.g., Mathematica cannot determine the zeros of this function. We emphasize that the number of zeros is not an input parameter of our method. Furthermore, we see that a step refinement as described in Section 4.2 was necessary for all functions. The number of (harmonic) Newton iterations also includes

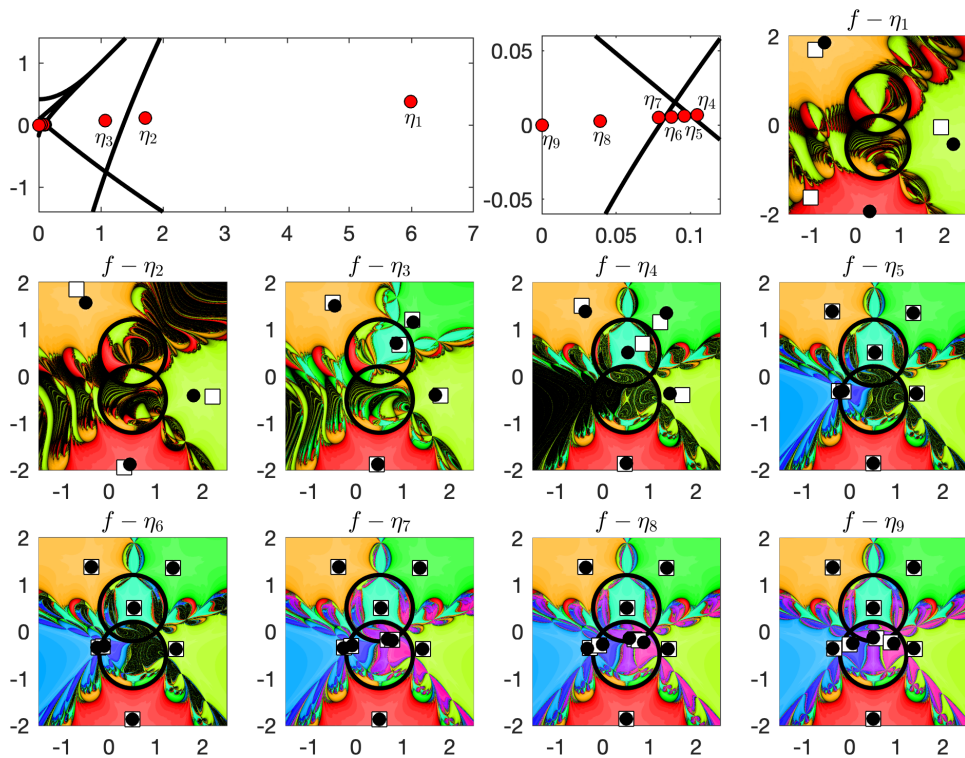


Figure 8: Transport of images method for (5.1) with $n = 3$: Transport path and basins of attraction of $H_{f-\eta_k}$ with prediction set (white squares) and zeros of $f - \eta_k$ (black dots).

iterations which were necessary to decide whether a step has to be refined.

Figure 8 illustrates the transport of images method for (5.1) with $n = 3$. Panel 1 and 2 display the transport path and a zoom in close to the origin. The remaining panels show the dynamics of the harmonic Newton maps $H_{f-\eta_k}$ for $k = 1, 2, \dots, 9$. Recall from Remark 3.8 that points which are attracted by the same solution have the same color. The initial phase is visualized in the top right plot. Every solution of $f(z) = \eta_1$ (black dots) attracts exactly one of the initial points (white squares), constructed as in Section 3.2, hence these initial points form a prediction set of $f^{-1}(\{\eta_1\})$. For aesthetic reasons, we set $\eta_1 = 6e^{i\pi/50}$ by hand. The remaining panels visualize the steps in the transport phase, again with the solutions of $f(z) = \eta_k$ (black dots) and the prediction sets (white squares). In particular, we see how the basins of attraction evolve while η_k “travels” along the transport path. New basins and their respective solutions appear in pairs for η_3 (green and cyan), η_5 (blue and light blue) and η_7 (pink and purple), right after a caustic crossing, as predicted by the theory. For each step, the prediction set of $f^{-1}(\{\eta_{k+1}\})$ consists of $f^{-1}(\{\eta_k\})$ (black dots in the previous panel), and of the points z_{\pm} from Theorem 3.5 in case of a caustic crossing. We

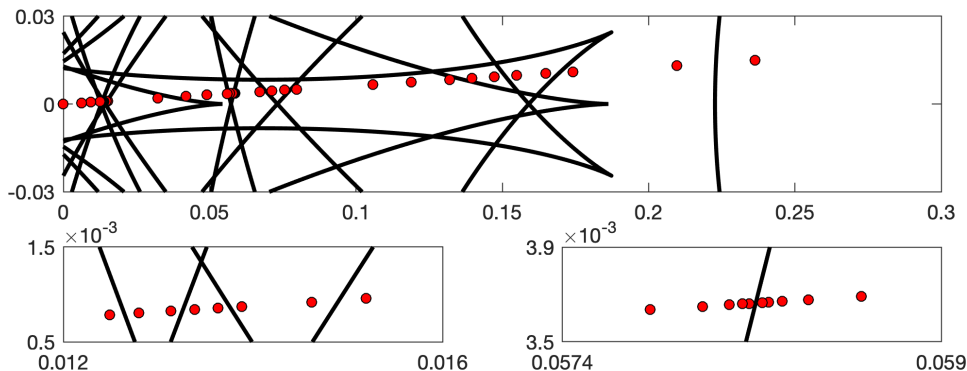


Figure 9: Transport path for (5.3) with $n = 7$, $\rho = 0.7$, $\varepsilon = 0.1$ and $\theta = \frac{\pi}{50}$.

see that the “new” solutions are close to the predicted points z_{\pm} . Note that Theorem 3.4 does not apply to the step from η_7 to η_9 . Therefore this step was divided by introducing the point $\eta_8 = (\eta_7 + \eta_9)/2$. A transport path with more step refinements, but for the function (5.3), is displayed in Figure 9.

Next, we compute the zeros of the function (5.2) for different values of n with the transport of images method (without fixing the angle θ). For each $n = 3, 4, \dots, 12$, we consider 50 instances of (5.2) with randomized $\rho \in [0.7, \rho_c[$, and apply our method to these functions. Similarly, we consider 50 instances of the function (5.3) with random $\rho \in [0.7, \rho_c[$ and $\varepsilon \in [\frac{\varepsilon^*}{2}, \frac{3\varepsilon^*}{4}]$. The quantities ρ and ε are uniformly distributed in the respective intervals. Table 2 shows the computed number of zeros, the number of harmonic Newton iterations, the number of restarts with a new angle θ , and the relative computation time of the caustics. For each n , the quantities are averaged over all instances. We observe the following. First of all, the transport of images method terminates with the correct number of zeros for all n and all instances. For most of the functions the transport along the first ray is already successful. For the remaining ones, a restart with a new angle is necessary to compute the zeros. Moreover, we see that the computation time of the caustics is significant for the overall computation time. This can be exploited when solving $f(z) = \eta_k$ for several $\eta_k \in \mathbb{C}$, which is a scenario in the astrophysical application in [25, Sect. 10.5].

In our next example, we consider (5.2) with $n = 100$ and $r = 0.94$, and (5.3) with $n = 25$, $r = 0.9$ and $\varepsilon = 0.4$. Note that every transport path along a ray R_{θ} intersects the caustics at least 100 times for the first function, and at least 50 times for the second function. The transport of images method computes all zeros in a few seconds on a standard computer; see Table 3. The residuals are close to the machine precision. In contrast to the examples in Table 2, 7 restarts with a new angle θ are necessary for (5.3) with $n = 25$. This is due to the extremely nested caustics; see Figure 10 (left and middle). The 125 zeros and 26 poles of the second function are

n	zeros	N.iter.	rest.	caus.	n	zeros	N.iter.	rest.	caus.
3	10	543.98	0.00	64%	3	15	948.46	0.00	59%
4	13	926.68	0.00	59%	4	20	1613.32	0.02	52%
5	16	1328.06	0.02	57%	5	25	2046.24	0.02	51%
6	19	1432.50	0.00	58%	6	30	3014.40	0.00	48%
7	22	1765.74	0.02	55%	7	35	3590.90	0.04	46%
8	25	2253.86	0.02	54%	8	40	4989.04	0.00	43%
9	28	2653.40	0.00	54%	9	45	5820.60	0.06	40%
10	31	3126.28	0.04	52%	10	50	6941.06	0.06	39%
11	34	3393.04	0.00	53%	11	55	8035.50	0.10	37%
12	37	3926.20	0.02	51%	12	60	9154.42	0.04	38%

Table 2: The transport of images method averaged over 50 instances. Left: (5.2) for $\rho \in [0.7, \rho_c[$. Right: (5.3) for $\rho \in [0.7, \rho_c[$ and $\varepsilon \in [\frac{\varepsilon^*}{2}, \frac{3\varepsilon^*}{4}]$. Number of harmonic Newton iterations (N.iter.), number of restarts with new angle θ (rest.), relative computation time for the caustics (caus.).

Function	zeros	max. res.	rest.	time
(5.2), $n = 100, \rho = 0.94$	301	6.4737e-16	0	5.36 s
(5.3), $n = 25, \rho = 0.9, \varepsilon = 0.4$	125	1.3552e-15	7	2.52 s

Table 3: Zero computation with the transport of images method.

displayed in a phase plot in Figure 10. In a phase plot of f , the complex plane is colored according to the phase $f(z)/|f(z)|$; see [34] for an extensive discussion of phase plots and their applications.

As mentioned in the introduction, we are not aware of any specialized software to compute *all* zeros of harmonic mappings. However, we compare our method with the `roots` command of Chebfun2³. Chebfun2 [33] is the state-of-the-art toolbox for numerical computation with (real or complex) smooth and bounded functions on a rectangle in the plane. We consider again the functions from Table 2. To compute the zeros of (5.2) and (5.3) with Chebfun2, we multiply them by their respective denominators to remove the poles, and thus obtain the functions

$$\begin{aligned}
F_1(z) &= z(\bar{z}^n - \rho^n) - \bar{z}^{n-1}, \\
F_2(z) &= (|z|^2 - 1)\bar{z}^n + (\varepsilon - |z|^2)\rho^n.
\end{aligned}$$

We apply Chebfun2 on the square $R = [-1.2, 1.2] \times [-1.2, 1.2]$, which contains all zeros of F_1 and F_2 for all $n = 3, 4, \dots, 12$ and all ρ and ε as above. Note that the supremum norm of F_j on R grows exponentially with n , which limits the accuracy that we can expect for growing n . Despite this difficulty, Chebfun2 computes all zeros of F_1 for all instances. For F_2 , Chebfun2 returns

³Chebfun2, www.chebfun.org, version of September 30, 2020.

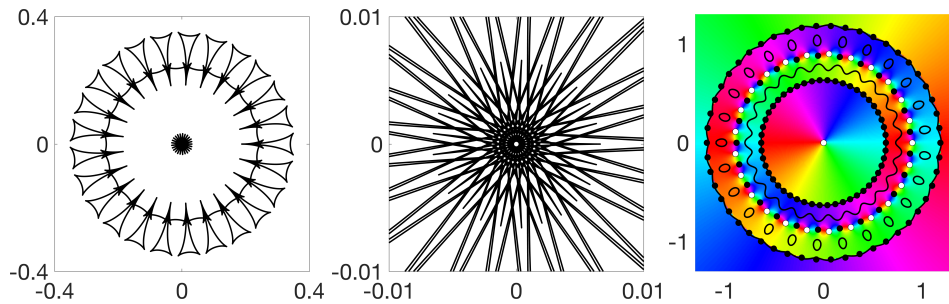


Figure 10: The harmonic mapping $f(z) = z - \left(0.6 \frac{z^{24}}{z^{25} - 0.925} + 0.4 \frac{1}{z}\right)$; see (5.3). Left: caustics. Middle: zoom of caustics. Right: phase plot with critical curves, zeros (black dots) and poles (white dots).

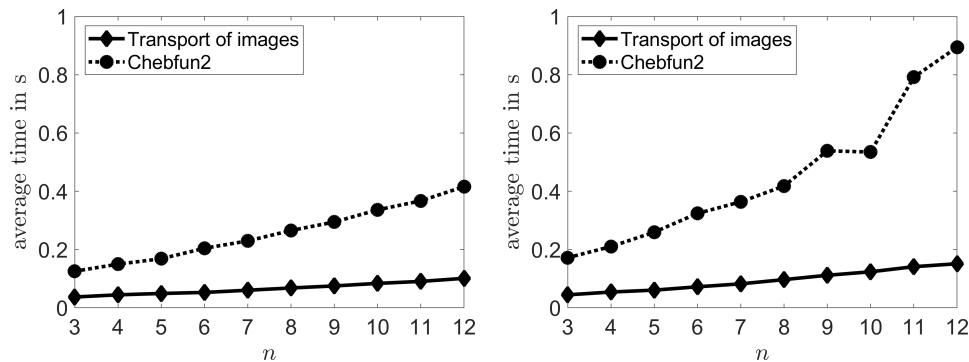


Figure 11: Timings of the transport of images method and Chebfun2 averaged over the 50 instances for (5.2) (left) and (5.3) (right) as in Table 2.

the correct number of zeros for all instances for $n = 3, 4, \dots, 9$ and $n = 11$. In contrast, Chebfun2 returns a wrong number of zeros for 5 out of 50 instances when $n = 10$ or $n = 12$. This highlights the ill-behavedness of the considered functions, and how difficult it is to compute their zeros. The problem adapted transport of images method finishes in all cases with the correct number of zeros; see Table 2. Moreover, it is much faster than Chebfun2 in this example; see Figure 11.

6 Summary and outlook

We established and analyzed the transport of images method, which is the first problem-adapted method to compute *all* zeros of a (non-degenerate) harmonic mapping f . Our method is guaranteed to find all zeros of f , even though this number is a priori unknown, as long as the number of zeros is finite. Moreover, our Matlab implementation performs remarkably well for several functions from the literature. While we focused on the computation

of zeros in our examples, we can also compute all solutions of $f(z) = \eta$ for any point $\eta \in \mathbb{C} \setminus f(\mathcal{C})$. For this, we either consider $f - \eta$, or replace the transport path from η_1 to 0 by a transport path from η_1 to η (with η_1 from the initial phase). More generally, we can compute all solutions of $f(z) = \eta$ given all solutions of $f(z) = \xi$ (with any points $\eta, \xi \in \mathbb{C} \setminus f(\mathcal{C})$) and the caustics of f , by transporting the solutions along a transport path from ξ to η . This allows us to deduce the solutions for all right hand sides from the local behavior of f on the critical curves.

Further studies of the transport of images method could include different constructions of transport paths, e.g., step size control, improvements of the computation of the caustics, as well as the investigation of other algorithms as corrector. Generalizing the transport of images method to a broader class of functions, e.g., for harmonic mappings on domains with boundary (see e.g. [4]), might also be of interest. Finally, adjusting the transport of images method to the special functions of gravitational lensing should be of particular interest.

Acknowledgements We thank Jörg Liesen for valuable comments on the manuscript.

References

- [1] E. L. ALLGOWER AND K. GEORG, *Introduction to numerical continuation methods*, vol. 45 of Classics in Applied Mathematics, Society for Industrial and Applied Mathematics (SIAM), Philadelphia, PA, 2003.
- [2] J. ARANGO, H. ARBELÁEZ, AND J. RIVERA, *Orientation at singularities of harmonic functions*, *Monatsh. Math.*, (2020).
- [3] C. BÉNÉTEAU AND N. HUDSON, *A survey on the maximal number of solutions of equations related to gravitational lensing*, in *Complex analysis and dynamical systems*, Trends Math., Birkhäuser/Springer, Cham, 2018, pp. 23–38.
- [4] W. BERGWELER AND A. EREMENKO, *On the number of solutions of a transcendental equation arising in the theory of gravitational lensing*, *Comput. Methods Funct. Theory*, 10 (2010), pp. 303–324.
- [5] P. M. BLEHER, Y. HOMMA, L. L. JI, AND R. K. W. ROEDER, *Counting zeros of harmonic rational functions and its application to gravitational lensing*, *Int. Math. Res. Not. IMRN*, (2014), pp. 2245–2264.
- [6] P. DUREN, *Harmonic mappings in the plane*, vol. 156 of Cambridge Tracts in Mathematics, Cambridge University Press, Cambridge, 2004.
- [7] P. DUREN, W. HENGARTNER, AND R. S. LAUGESSEN, *The argument principle for harmonic functions*, *Amer. Math. Monthly*, 103 (1996), pp. 411–415.
- [8] C. D. FASSNACHT, C. R. KEETON, AND D. KHAVINSON, *Gravitational lensing by elliptical galaxies, and the Schwarz function*, in *Analysis and mathematical physics*, Trends Math., Birkhäuser, Basel, 2009, pp. 115–129.
- [9] L. GEYER, *Sharp bounds for the valence of certain harmonic polynomials*, *Proc. Amer. Math. Soc.*, 136 (2008), pp. 549–555.

- [10] W. HENGARTNER AND G. SCHÖBER, *Univalent harmonic functions*, Trans. Amer. Math. Soc., 299 (1987), pp. 1–31.
- [11] P. HENRICI, *Applied and computational complex analysis. Vol. 3*, Pure and Applied Mathematics (New York), John Wiley & Sons, Inc., New York, 1986.
- [12] D. KHAVINSON AND E. LUNDBERG, *Transcendental harmonic mappings and gravitational lensing by isothermal galaxies*, Complex Anal. Oper. Theory, 4 (2010), pp. 515–524.
- [13] D. KHAVINSON AND G. NEUMANN, *On the number of zeros of certain rational harmonic functions*, Proc. Amer. Math. Soc., 134 (2006), pp. 1077–1085.
- [14] D. KHAVINSON AND G. NEUMANN, *From the fundamental theorem of algebra to astrophysics: a “harmonious” path*, Notices Amer. Math. Soc., 55 (2008), pp. 666–675.
- [15] D. KHAVINSON AND G. ŚWIĄTEK, *On the number of zeros of certain harmonic polynomials*, Proc. Amer. Math. Soc., 131 (2003), pp. 409–414.
- [16] S.-Y. LEE, A. LERARIO, AND E. LUNDBERG, *Remarks on Wilmschurst’s theorem*, Indiana Univ. Math. J., 64 (2015), pp. 1153–1167.
- [17] J. LIESEN AND J. ZUR, *How constant shifts affect the zeros of certain rational harmonic functions*, Comput. Methods Funct. Theory, 18 (2018), pp. 583–607.
- [18] J. LIESEN AND J. ZUR, *The maximum number of zeros of $r(z) - \bar{z}$ revisited*, Comput. Methods Funct. Theory, 18 (2018), pp. 463–472.
- [19] R. LUCE, O. SÈTE, AND J. LIESEN, *Sharp parameter bounds for certain maximal point lenses*, Gen. Relativity Gravitation, 46 (2014), pp. 1–16.
- [20] R. LUCE, O. SÈTE, AND J. LIESEN, *A note on the maximum number of zeros of $r(z) - \bar{z}$* , Comput. Methods Funct. Theory, 15 (2015), pp. 439–448.
- [21] A. LYZZAIK, *Local properties of light harmonic mappings*, Canad. J. Math., 44 (1992), pp. 135–153.
- [22] S. MAO, A. O. PETTERS, AND H. J. WITT, *Properties of point mass lenses on a regular polygon and the problem of maximum number of images*, in The Eighth Marcel Grossmann Meeting, Part A, B (Jerusalem, 1997), World Sci. Publ., River Edge, NJ, 1999, pp. 1494–1496.
- [23] G. NEUMANN, *Valence of complex-valued planar harmonic functions*, Trans. Amer. Math. Soc., 357 (2005), pp. 3133–3167.
- [24] A. O. PETTERS, *Gravity’s action on light*, Notices Amer. Math. Soc., 57 (2010), pp. 1392–1409.
- [25] P. SCHNEIDER, J. EHLERS, AND E. E. FALCO, *Gravitational Lenses*, Springer Science & Business Media, Berlin Heidelberg, 1999.
- [26] O. SÈTE, R. LUCE, AND J. LIESEN, *Creating images by adding masses to gravitational point lenses*, Gen. Relativity Gravitation, 47 (2015), pp. Art. 42, 8.
- [27] O. SÈTE, R. LUCE, AND J. LIESEN, *Perturbing rational harmonic functions by poles*, Comput. Methods Funct. Theory, 15 (2015), pp. 9–35.
- [28] O. SÈTE AND J. ZUR, *Number and location of pre-images under harmonic mappings in the plane*, ArXiv e-prints: 1908.08759, (2019). To appear in Ann. Acad. Sci. Fenn. Math.
- [29] O. SÈTE AND J. ZUR, *A Newton method for harmonic mappings in the plane*, IMA J. Numer. Anal., 40 (2020), pp. 2777–2801.
- [30] T. SHEIL-SMALL, *Complex Polynomials*, vol. 75 of Cambridge Studies in Advanced Mathematics, Cambridge University Press, Cambridge, 2002.

- [31] S. SMALE, *Newton's method estimates from data at one point*, in The merging of disciplines: new directions in pure, applied, and computational mathematics (Laramie, Wyo., 1985), Springer, New York, 1986, pp. 185–196.
- [32] T. J. SUFFRIDGE AND J. W. THOMPSON, *Local behavior of harmonic mappings*, Complex Variables Theory Appl., 41 (2000), pp. 63–80.
- [33] A. TOWNSEND AND L. N. TREFETHEN, *An extension of Chebfun to two dimensions.*, SIAM J. Sci. Comput., 35 (2013), pp. c495–c518.
- [34] E. WEGERT, *Visual complex functions. An introduction with phase portraits.*, Birkhäuser/Springer Basel AG, Basel, 2012.
- [35] A. S. WILMSHURST, *The valence of harmonic polynomials*, Proc. Amer. Math. Soc., 126 (1998), pp. 2077–2081.